Hyperspectral Image Super Resolution Using Anomaly Weighted Gabor Based CNN

Ali Farajzadeh [iD]
Department of Electrical Engineering
University of Zanjan
Zanjan, Iran
a.farajzadeh@znu.ac.ir

Maryam Imani* [iD]
Faculty of Electrical and Computer Engineering
Tarbiat Modares University
Tehran, Iran
maryam.imani@modares.ac.ir

Shahram Mohammadi [iD]
Department of Electrical Engineering
University of Zanjan
Zanjan, Iran
shahram@znu.ac.ir

Abstract—**Hyperspectral images have high spectral resolution. But, due to the tradeoff between spectral and spatial resolution and various hardware constraints, imaging a hyperspectral image with high spatial resolution is not practical. Hyperspectral super resolution is a soft approach to solve this challenge. Recently, deep learning based methods such as convolutional neural network (CNN) show great success in this field. But, the contextual details in object boundaries and anomalies present in the scene are not well addressed. To this end, a new CNN based framework is proposed for hyperspectral image super resolution in this work. To improve ability of the convolutional blocks in simultaneous extraction of spectral and spatial characteristics, the weighted Gabor features are concatenated in output of the defined convolutional blocks. To extract more details containing anomalous targets present in the scene, the anomaly scores of pixels are calculated and used for weighting the Gabor features. The experiments on three real hyperspectral images acquired by AVIRIS and ROSIS sensors show superior performance of the proposed framework compared to several state-of-the-art methods based on CNN and residual networks. In addition to common super resolution metrics such as SAM and ERGAS, the efficiency of different methods are evaluated according to the classification accuracy metrics such as overall accuracy and kappa coefficient. The overall classification accuracy is increased from 70.39 to 88.23 in Indian dataset, from 86.07 to 96.20 in Pavia University dataset, and from 95.82 to 99.12 in Pavia center dataset.**

Keywords: super resolution, hyperspectral image, anomaly, CNN.

---

* Corresponding Author

I. INTRODUCTION

Hyperspectral images provide a rich source of spectral information needed for various applications such as scene classification, target detection and environmental monitoring [1]. But, due to imperfect imaging sensors, acquiring images with both high spectral and spatial resolutions is not possible. So, spatial resolution enhancement of hyperspectral images is a hot topic in remote sensing field [2].

Various hyperspectral super resolution techniques have been suggested to reconstruct a high resolution hyperspectral image from a low resolution one. Generally, there are two categories of super resolution methods. In the first category, it is tried that with fusing a hyperspectral image with a high spatial resolution image (panchromatic, RGB or multispectral), the spatial resolution of the hyperspectral image is increased [3]-[4]. Different fusion methods such as tensor factorization [5], sparse representation and dictionary learning [6], component substitution [7] and multi-resolution analysis approaches [8] belong to the first category. In the second category, there is no auxiliary image for hyperspectral super resolution. Different interpolation [9] and learning based approaches [10] belong to the second category. Recently, deep learning methods such as convolutional neural networks (CNNs) [11]-[12], due to their abilities in extraction of robust features invariant to local changes, and autoencoders [13] have shown great success for hyperspectral super resolution due to their abilities in extraction of robust features invariant to local changes.

A three layers CNN is suggested for hyperspectral super resolution in [14] where the network is followed by a triplet-pipline CNN for hyperspectral classification. Three coupled autoencoders are used for fusion of hyperspectral and multispectral images through unmixing them to their endmembers and abundances. In [15], the wavelet transformation is used to decompose the hyperspectral image into its frequency components. Then, the obtained components are fed to three branches of three dimensional CNNs. The observation matrix of hyperspectral image is represented by subnetworks and taken into account for an end-to-end optimization through a model guided convolutional network in [16].

Gabor filters with acquiring optimal localization characteristics in both frequency and spatial domains can be a good candidate for hyperspectral feature extraction resulting in contextual features containing details with spectral fidelity [17]-[18]. The use of Gabor filters beside the CNNs is suggested for hyperspectral image analysis in several works [19]-[20].

In this work, two improved Gabor based convolutional based networks are proposed for hyperspectral super resolution. In addition to texture and objet boundaries, there are some anomalies in a hyperspectral image. Detection of these anomalies is important to appropriately extract details for super resolution. To this end, the Gabor features are weighted with anomaly scores calculated from the local regions with assumption of multivariate normal distribution for the background image. Anomaly weighted Gabor based CNN (AGCNN) and anomaly weighted and edge based Gabor CNN (AEGCNN) are proposed according to this idea. The experiments on three real hyperspectral images show good performance of the proposed methods with respect to several competitors with a significant difference.

II. THE ANOMALY WEIGHTED GABOR BASED CNN

A. The Proposed network

A convolution based neural network consisting of convolutional blocks and Gabor feature maps revised by anomaly scores is proposed for hyperspectral super resolution in this work.

Generally CNNs provide hierarchical representation of the given input by applying the convolutional learnable filters for local feature extraction. CNNs with two useful characteristics of shared weights and local connections are appropriate feature extractors for hyperspectral images. However, when a CNN is used for hyperspectral super resolution, it may be not efficient enough for extraction of image details. In addition, due to hyperparameters in a CNN and low number of labeled samples for training, the used CNN cannot have high depth.

To deal with these difficulties, injection of desired feature cubes to the output of convolutional layers is suggested. The blockdiagram of the proposed network is shown in Fig 1. Each ConvRD block consists of two convolutional layers, each one followed by the rectified linear unit (ReLu) and dropout layer with dropping probability of 0.2. The first convolutional layer contains 4 kernels and the second one contains d kernels where d denotes the number of spectral bands, and all convolutional kernels are from size of 3×3. The last ConvRD block contains 16 and 32 filters, respectively in its first and second convolutional kernels, respectively. Low resolution hyperspectral image (LR HSI) patch is given as input and the high resolution (HR) HSI pixel is achieved in the output. The edge feature cube and the anomaly weighted Gabor feature cube extracted by the HR HSI are added and concatenated to the output of three first ConvRD blocks in the training process.

The ReLu layer is used as the nonlinear activation function, which is efficient for learning the nonlinear representation of the hyperspectral image and avoiding the vanishing gradient issue. The dropout layer with dropping probability of $p = 0.2$ is also used to avoid the overfitting. The output of ConvRD block is obtained by:

$$F^l = \text{Drop}_p\big(\mathcal{R}(F^{l-1} * W^l + b^l)\big) \qquad (1)$$

where F^l is the output feature map in lth layer, W^l and b^l are the learnable weights and bias parameters in

layer l, $\mathcal{R}$ is the nonlinear ReLu activation function and Drop_p is the droput function with dropping probability of p.

Two networks are proposed in this work. Anomaly weighted Gabor based CNN (AGCNN) and anomaly weighted and edge based Gabor CNN (AEGCNN). In AGCNN, the Gabor feature cubes weighted by anomaly scores are concatenated in output of the ConvRD blocks. In AEGCNN, before concatenating the anomaly weighted Gabor feature cube, the edge feature maps extracted by an edge detector such as 'Sobel' are added to the ConvRD outputs. The edge detector is applied to each band of the hyperspectral image. The edge cube is added to the convolutional outputs to help the network to learn more object boundaries.

B. Gabor features

Gabor functions inspired from the visual context of human act as low level texture and oriented edge discriminators. The Gabor functions are sensitive to various scale information and different frequencies. Gabor filters achieve optimal resolution in both frequency and spatial domains. Spatial resolution as a measure of finesse or coarseness of an image determines the amount of details in the image. From the other hand, spectral resolution is ability of the imaging sensor for small differences detection in wavelength. Due to providing optimal resolution in both spectral and spatial dimensions, Gabor filters can be useful tools for feature extraction in hyperspectral super resolution applications.

The output of a Gabor filter is a complex value. While the amplitude contains information about directional frequency spectrum, the phase provides location of details and edges in the processed image. A Gabor filter is obtained by modulation of a sinusoidal function with a Gaussian overlap as follows [26]:

$$H(x,y) = \exp\left(-\frac{\acute{x}^2 + \gamma^2 \acute{y}^2}{2\sigma^2}\right) \times \exp\left(j\left(2\pi\frac{\acute{x}}{\lambda} + \psi\right)\right) \quad (2)$$

where

$$\acute{x} = x\cos(\theta) + y\sin(\theta) \quad (3)$$
$$\acute{y} = -x\sin(\theta) + y\cos(\theta) \quad (4)$$

where γ denotes the spatial aspect ratio, σ determines the width of the Gaussian envelop, λ is the wavelength, ψ represents the phase offset and θ is the separation angle. To apply a Gabor filter bank with N_s scales and N_d directions to a hyperspectral image, at first, the hyperspectral dimensionality is reduced by the principal component transform. The Gabor filter bank is applied to the m first principal components. Then, the outputs are concatenated to form the Gabor feature cube. The magnitude of convolution of each Gabor filter $H(x,y)$ with each principal component $I(x,y)$ is considered as a Gabor feature map in the output:

$$G(x,y) = |H(x,y) * I(x,y)| \quad (5)$$

C. The Anomaly weighted Gabor

Although texture characteristics extracted by Gabor filters contain information about contextual details of the input image, but there are some anomalies in the

hyperspectral images, which may be ignored in the Gabor filtering process. With inspiration from the Reed-Xiaoli (RX) detector [21], the probability value of anomaly for each pixel is calculated and used as a weight for Gabor features of the given pixel. Some pixels of the hyperspectral image having two characteristics are considered as anomalies: 1-pixels with different spectral signatures with respect to the background, and 2-pixels with low probability occurrence. Let assume that the hyperspectral background follows a multivariate Gaussian distribution. In this case, pixel $\boldsymbol{x}$ belongs to the background with the following probability [21], [27]:

$$p(\boldsymbol{x}/B) = \frac{1}{\sqrt{(2\pi)^d|\boldsymbol{C}|}} \exp\left[-\frac{1}{2}(\boldsymbol{x}-\boldsymbol{\mu})^T\boldsymbol{C}^{-1}(\boldsymbol{x}-\boldsymbol{\mu})\right] \quad (6)$$

where d is the number of hyperspectral bands, $\boldsymbol{\mu}$ and $\boldsymbol{C}$ are the mean vector and covariance of the background image. An anomalous pixel is significantly far from the background. So, if $\boldsymbol{x}$ is an anomaly, $p(\boldsymbol{x}/B)$ will be very small and thus, $(\boldsymbol{x}-\boldsymbol{\mu})^T\boldsymbol{C}^{-1}(\boldsymbol{x}-\boldsymbol{\mu})$ has a large value for an anomaly. To score pixels of a hyperspectral image according to their anomaly probabilities, the following anomaly distance is defined [28]:

$$d_i = (\boldsymbol{x}_i - \boldsymbol{\mu}_w)^T(\boldsymbol{C}_w + \delta\boldsymbol{I})^{-1}(\boldsymbol{x}_i - \boldsymbol{\mu}_w) \quad (7)$$

where $\boldsymbol{x}_i \in \mathcal{R}^d; i = 1,2,\dots,N$ is i th pixel of the hyperspectral image, N is the total number of pixels and, $\boldsymbol{\mu}_w$ and $\boldsymbol{C}_w$ are the mean vector and covariance matrix calculated in a local window with size of $L \times L$ centered in $\boldsymbol{x}_i$, $\boldsymbol{I}$ denotes the identity matrix with $d \times d$ dimensions and δ is the regularization parameter. To include the spatial information of neighborhood, the local mean and covariance statistics are used instead of the global ones. In addition, due to high dimensionality of the hyperspectral image and to deal with the singularity problem, the regularized covariance matrix, i.e., $\boldsymbol{C}_w + \delta\boldsymbol{I}$ is used instead of $\boldsymbol{C}_w$. $d_i = d(p_i, q_i)$ is the anomaly score of pixel $\boldsymbol{x}_i$ with spatial coordinate of (p_i, q_i), which can be used as a weight for output of the Gabor filter as follows:

$$G_w(p_i, q_i) = d(p_i, q_i) \times G(p_i, q_i) \quad (8)$$

where $G(p_i, q_i)$ and $G_w(p_i, q_i)$ are the Gabor feature and the weighted Gabor feature, respectively in the pixel position (p_i, q_i).

III. EXPERIMENTS

A. Datasets, competitors and parameter settings

Three hyperspectral images are used for super resolution experiments. The first dataset is the Indian Pines collected by Airborne Visible-Infrared Imaging Spectrometer (AVIRIS) in 1992 over Northwestern Indiana. It has 145×145 pixels and 224 spectral bands in wavelength of 0.4 to 2.5 μm. After discarding water absorption channels, 200 spectral bands are selected. The spatial resolution of it is 20 m by pixel. The second and third hyperspectral images with 115 original spectral channels are acquired by the Reflective Optics System Imaging Spectrometer (ROSIS) with 1.3 m by

pixel. After discarding the noisy channels, 103 and 102 bands are remained for Pavia University and Pavia center datasets, respectively.

The original Pavia University dataset has 610×340 pixels and Pavia center has 1096×715 pixels. A sub image of Pavia University with size of 200 × 130 containing 7 land cover classes and a sub image of Pavia center with size of 202×152 containing 5 land cover classes are used for doing experiments. 50% data samples are used as training and the remained samples are used as testing set in each dataset. 50% of data is equal to 10513 samples in Indian, 13000 samples in Pavia University and 15352 samples in Pavia center dataset.
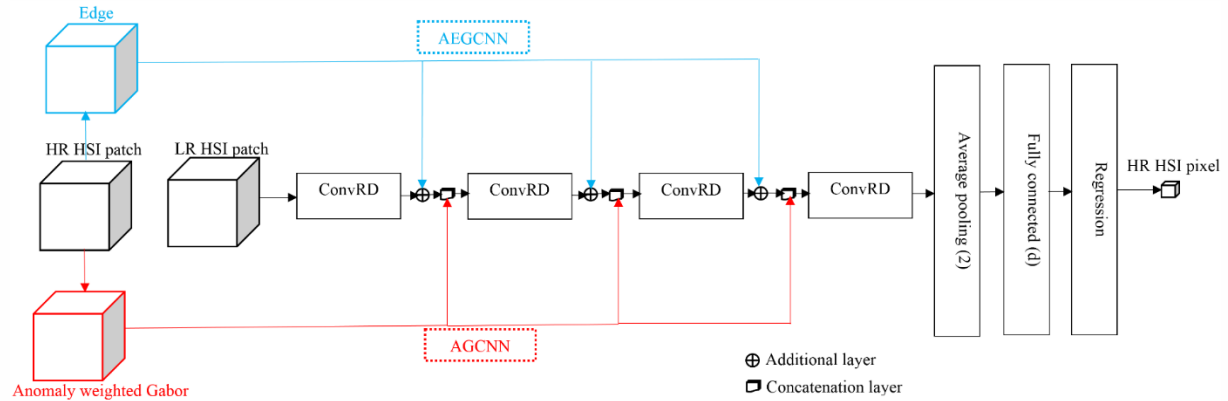

Figure 1. Fig. 1. Blockdiagram of the proposed AGCNN and AEGCNN networks.

TABLE I. THE SUPER RESOLUTION RESULTS FOR INDIAN DATASET.

	MSSIM (1)	PSNR (+∞)	SAM (0)	ERGAS (0)	RMSE (0)	UIQI (1)
CNN	0.57	33.63	9.11	0.61	3.66	0.82
RES	0.66	33.46	7.65	0.53	3.17	0.91
ECNN	0.54	33.38	9.09	0.66	3.97	0.82
GCNN	0.71	35.58	7.39	0.33	1.98	0.95
EGCNN	0.69	35.36	7.44	0.35	2.10	0.94
AGCNN	0.74	35.34	7.67	0.36	2.15	0.95
AEGCNN	0.74	35.29	7.44	0.35	2.12	0.95

TABLE II. THE SUPER RESOLUTION RESULTS FOR PAVIA UNIVERSITY DATASET.

	MSSIM (1)	PSNR (+∞)	SAM (0)	ERGAS (0)	RMSE (0)	UIQI (1)
CNN	0.46	7.34	6.38	3.65	58.87	0.55
RES	0.77	13.02	5.24	1.59	24.93	0.92
ECNN	0.44	7.28	6.35	3.76	60.57	0.53
GCNN	0.51	8.10	6.17	3.27	51.99	0.60
EGCNN	0.44	7.51	6.33	3.66	59.23	0.49
AGCNN	0.80	13.62	5.11	1.47	23.15	0.91
AEGCNN	0.81	13.78	5.04	1.37	21.89	0.93

TABLE III. TABLE 3. THE SUPER RESOLUTION RESULTS FOR PAVIA CENTER DATASET.

	MSSIM (1)	PSNR (+∞)	SAM (0)	ERGAS (0)	RMSE (0)	UIQI (1)
CNN	0.51	10.41	6.04	2.44	37.49	0.67
RES	0.75	13.98	4.69	1.46	22.43	0.92
ECNN	0.58	12.54	6.08	1.89	29.00	0.76
GCNN	0.65	13.60	5.24	1.57	24.05	0.86
EGCNN	0.64	13.17	5.74	1.66	24.92	0.83
AGCNN	0.85	16.45	3.93	0.78	11.91	0.98
AEGCNN	0.83	16.29	3.94	0.90	14.00	0.97

For doing experiments, the original hyperspectral images are considered as HR images and the down sampled versions of them are considered as LR images. The downsampling is implemented by applying an antialiasing filter followed by downsampling along both the vertical and horizontal dimensions with the scaling factor of 2. The bicubic interpolation is used for resizing the image. A 11 × 11 lowpass filter with Hamming window is used to avoid aliasing.

So far, various versions of CNN and residual (RES) learning based networks have been proposed for hyperspectral image super resolution [22]-[25]. So, a specific version of CNN and RES are used as the competitors here. In addition to CNN and RES, different cases of the suggested framework called as edge based CNN (ECNN) and Gabor based CNN (GCNN) are also experimented to show impact of each part of the proposed framework. In this work, to have a fair comparison among the proposed method and the

competitors, the same base structure for all deep learning methods are used for doing experiments. The proposed methods (AGCNN and AEGCNN) are compared with CNN, residual network (RES), ECNN, GCNN and EGCNN. To have a fair comparison between the networks, the same structure is used for all of them as shown in Fig. 1. In other words, the experimented CNN has the same structure of Fig. 1 without any injected feature cubes through addition or concatenation layers; RES has the general structure shown in Fig. 1 where the original input patch is added to the output of each ConvRD block. In ECNN, the edge feature cube is added to the output of the ConvRD blocks; and in GCNN, the conventional Gabor feature are concatenated to the output of the ConvRD blocks. EGCNN uses both edge and conventional Gabor feature cubes.

The input of all networks are the patch images with size of 5×5. In the anomaly weighted Gabor filters, $L = 7$ is used as size of the local window. The appropriate values of patch size and local window size can be obtained through doing experiments for each dataset. In this work, to avoid parameter settings for each dataset, the patch size of 5×5 and local window of $L = 7$ are chosen for all hyperspectral images. According to done experiments, these parameters' values are relatively appropriate for both AVIRIS dataset with spatial resolution of 20m by pixel and ROSIS datasets with a spatial resolution of 1.3m per pixel. These parameters are chosen as a tradeoff between accuracy and complexity. With selection of a small patch or local window, low spatial information are contributed in the super resolution process and with considering large patch or local window, redundant or non-related spatial information may be included in the decision process. In addition, larger window size leads to increasing the complexity burden.

$\delta = 10^{-4}$ is used as the regularization parameter. $m = 3$ principal components of the hyperspectral images are used for Gabor feature extraction. The Adam optimizer is used for training of the networks with 20, 30 and 50 epochs for Indian, Pavia University and Pavia center datasets, respectively.

B. Performance assessment with super resolution metrics

To assess quality of the generated high resolution images, the following quantity measures are used: mean structural similarity index (MSSIM), peak signal to noise ratio (PSNR), spectral angle mapper (SAM), Error relative dimensionless global error in synthesis (ERGAS), root mean square error (RMSE), and universal image quality index (UIQI). The obtained results for Indian, Pavia University and Pavia center datasets are reported in Tables 1-3, respectively where the ideal value of each measure is represented in the parentheses. A sample band of the reconstructed hyperspectral images are also shown in Figs. 2-4. The following conclusions can be found from the achieved results:

1- In all datasets, CNN obtains the lowest performance in terms of all evaluation measures. It represents that the convolutional kernels are not lonely enough for extraction of the image details.

2- Two proposed AGCNN and AEGCNN are two best methods with a significant difference compared to other methods. The Gabor features weighted by defined anomaly scores contain rich contextual information with highlighting anomalies in local regions, which are so efficient for hyperspectral super resolution.
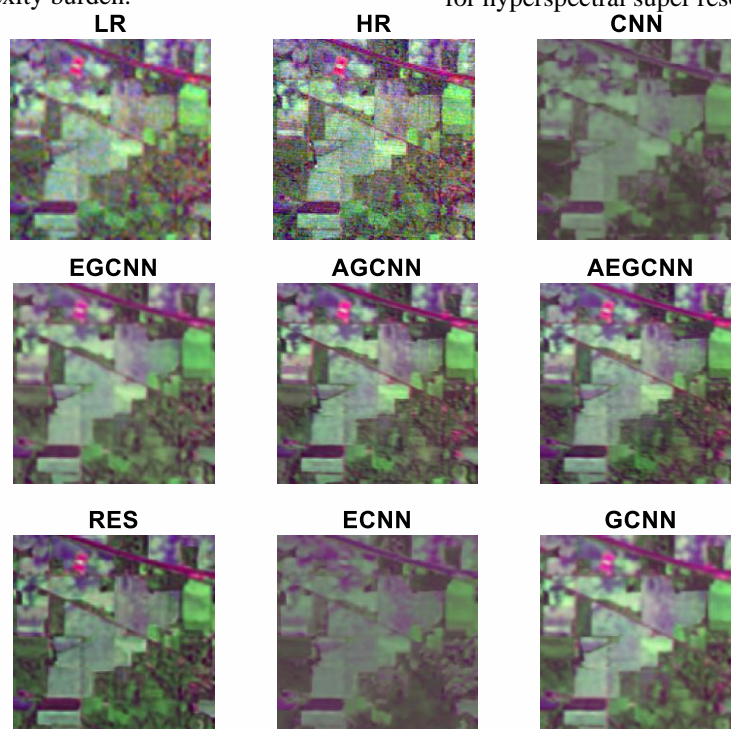

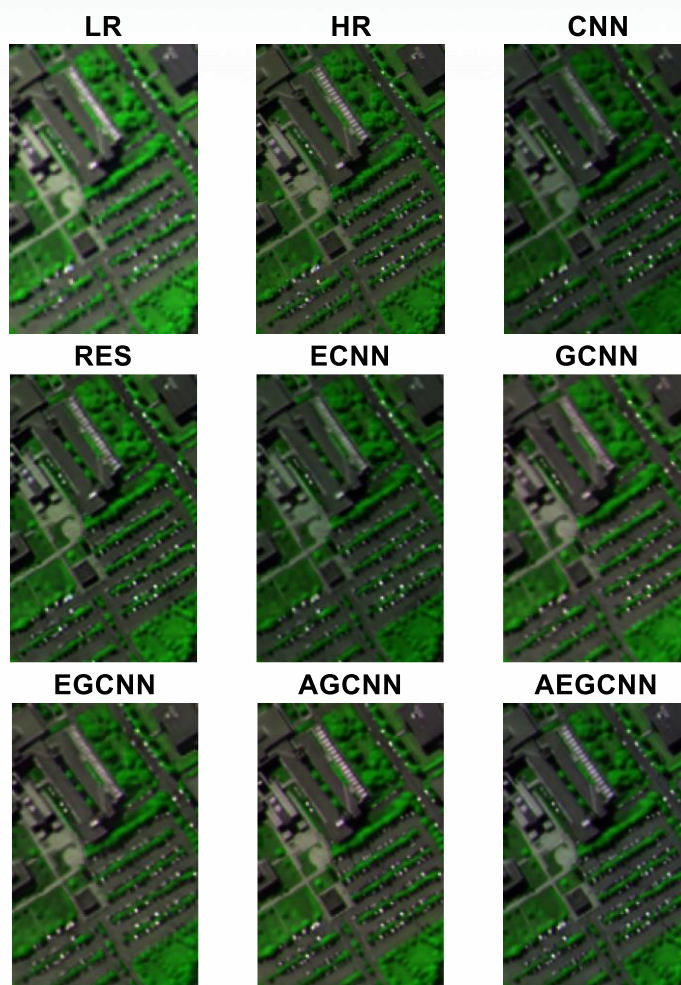Figure 2.   Fig. 2. The super resolution images for Indian dataset.

Figure 3.   Fig. 3. The super resolution images for Pavia University dataset.
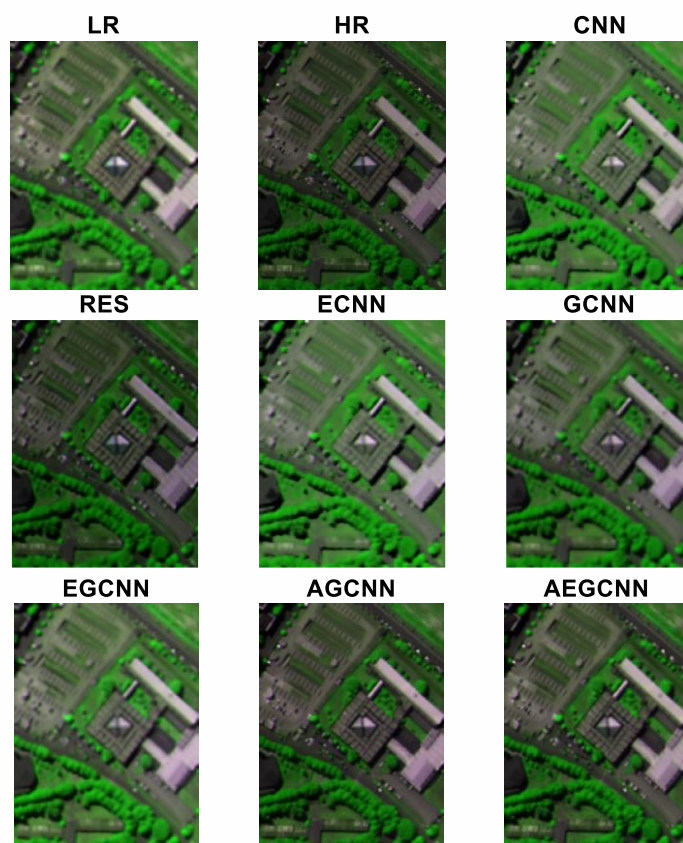

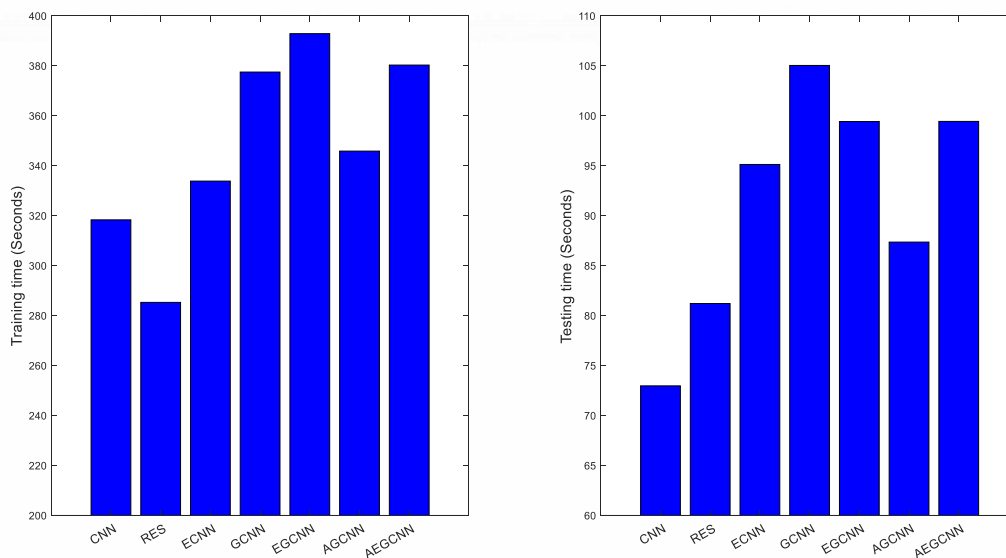Figure 4.   The super resolution images for Pavia Center dataset.

Figure 5. The training and testing time of super resolution methods.

TABLE IV. THE CLASSIFICATION RESULTS FOR INDIAN DATASET.

No.	Name of class	# samples	Raw	CNN	RES	ECNN	GCNN	EGCNN	AGCNN	AEGCNN
1	Corn-no till	1434	66.32	61.09	78.73	55.02	81.59	81.73	89.19	84.73
2	Corn-min till	834	72.06	49.04	79.26	40.29	81.89	86.21	90.05	86.57
3	Grass/pasture	497	91.55	75.25	90.95	77.87	89.34	90.34	92.76	94.16
4	Grass/trees	747	92.50	76.84	93.57	81.12	96.92	93.44	97.72	96.25
5	Hay-windrowed	489	98.98	95.50	99.80	97.96	99.18	97.55	98.98	98.57
6	Soybeans-no till	968	71.80	39.67	80.17	48.97	80.27	86.26	93.90	88.02
7	Soybeans-min till	2468	47.29	51.13	70.54	40.11	70.91	74.43	82.98	80.43
8	Soybeans-clean till	614	76.87	6.51	76.38	17.43	84.04	83.22	90.88	86.81
9	Woods	1294	79.52	62.52	79.91	75.73	88.18	90.80	96.37	95.98
10	Bldg-Grass-Tree-Drives	380	78.95	53.68	86.05	63.16	97.37	94.47	96.32	95.26
	Average Accuracy (%)		77.58	57.12	83.54	59.77	86.97	87.85	92.91	90.68
	Overall Accuracy (%)		70.39	55.52	79.96	55.40	82.88	84.65	90.83	88.23
	Kappa Coefficient		0.6638	0.4896	0.7699	0.4915	0.8037	0.8239	0.8944	0.8644

TABLE V. THE CLASSIFICATION RESULTS FOR PAVIA UNIVERSITY DATASET.

Name of class	# samples	Raw	CNN	RES	ECNN	GCNN	EGCNN	AGCNN	AEGCNN
Asphalt	317	90.22	74.76	86.75	70.35	89.59	93.69	85.49	96.21
Meadows	617	97.41	99.84	99.51	98.54	99.51	99.51	99.84	99.03
Gravel	966.	78.57	88.61	89.96	74.74	91.41	88.51	97.72	95.96
Trees	263	96.20	96.20	96.96	94.68	97.72	98.10	96.96	95.44
Bitumen	424	96.46	89.62	94.58	88.44	97.17	94.34	94.81	97.64
Self-Blocking Bricks	1641	78.61	48.39	80.62	51.13	89.21	89.34	92.26	94.33
Shadows	293	100.00	99.66	100.00	100.00	100.00	99.32	100.00	100.00
Average Accuracy (%)		91.07	85.30	92.63	82.55	94.94	94.69	95.30	96.95
Overall Accuracy (%)		86.07	75.82	89.14	73.19	93.05	92.48	95.00	96.20
Kappa Coefficient		0.8245	0.7013	0.8630	0.6673	0.9122	0.9050	0.9365	0.9516

TABLE VI. THE CLASSIFICATION RESULTS FOR PAVIA CENTER DATASET.

| Name of class	# samples	Raw	CNN	RES	ECNN	GCNN	EGCNN	AGCNN	AEGCNN
Trees	490	99.80	100.00	99.39	100.00	100.00	100.00	99.39	100.00
Meadows	58	100.00	100.00	100.00	100.00	100.00	100.00	100.00	100.00
Bricks	2001	93.95	98.05	94.25	97.75	97.95	98.90	98.50	98.85
Bare Soil	370	95.68	96.76	99.46	99.73	98.65	96.49	97.30	98.65
Asphalt	477	99.16	99.58	99.37	100.00	100.00	100.00	97.90	99.58
Average Accuracy (%)		97.72	98.88	98.49	99.50	99.32	99.08	98.62	99.42
Overall Accuracy (%)		95.82	98.44	96.38	98.65	98.65	98.97	98.44	99.12
Kappa Coefficient		0.9321	0.9742	0.9412	0.9777	0.9776	0.9829	0.9741	0.9854
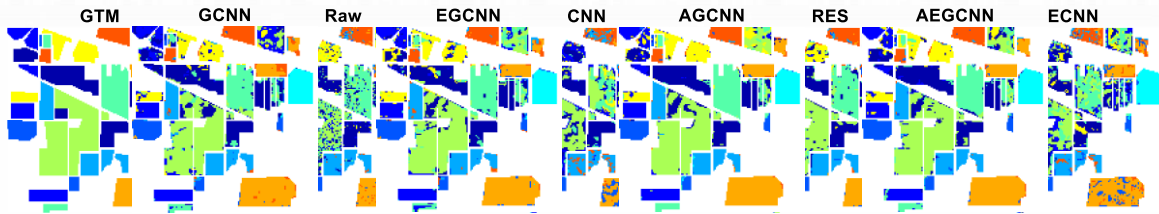
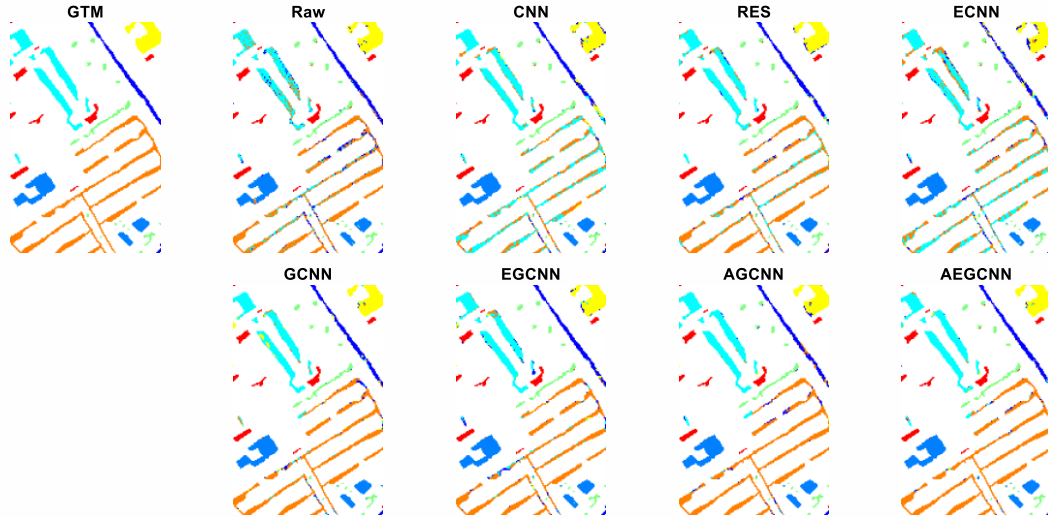Figure 6.   The classification maps for Indian dataset.

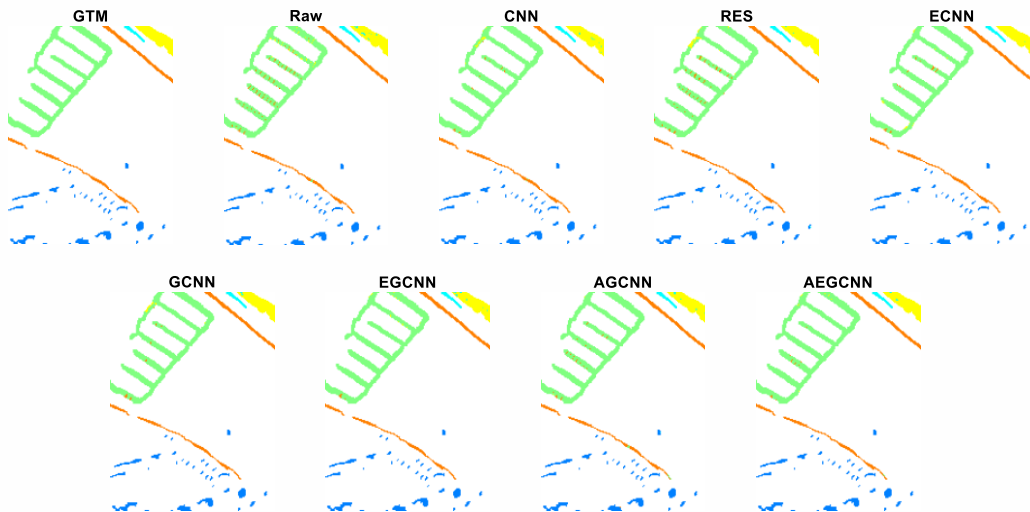Figure 7.   The classification maps for Pavia University dataset.

Figure 8.   The classification maps for Pavia Center dataset.

3- In Indian dataset, GCNN ranks third after AGCNN and AEGCNN while in two other datasets, RES provides the best performance after the proposed methods.

4- In Indian dataset, the use of edge feature cube has not positive effect in images reconstructed by CNN and GCNN. In other words, generally CNN works better than ECNN and GCNN works better than EGCNN. But, in the proposed methods, the use of edge cube leads to better performance from the SAM, ERGAS and RMSE point of view. This improvement can be seen in comparison between AGCNN and AEGCNN.

5- In Pavia University, the use of edge cubes degrades performance of ECNN compared to CNN, and performance of EGCNN compared to GCNN. But, the results show improvement of AEGCNN compared to AGCNN. It can be found

that in Pavia University image, the use of edge features together with the conventional Gabor features is not appropriate. But, when they are used together with the revised Gabor features weighted by anomaly scores lead to increasing the spatial resolution and spectral fidelity.

6- In Pavia center dataset, the use of edges is useful just for improvement of CNN.

The training time and testing time of different methods are compared together in Fig. 5. The highest training time is related to EGCNN and AEGCNN while the lowest training time is related to RES. GCNN, AEGCNN and EGCNN have the highest running time in the testing phase. Computations related to calculating the edges, Gabor feature maps and anomaly scores lead to increasing the running time.

C. Performance assessment with classification metrics

To assess performance of different super resolution methods from the land cover classification accuracy point of view, the produced hyperspectral images with increased resolution are given as input of the support vector machine (SVM) for doing the classification task. The SVM classifier is implemented in LIBSVM [29] with polynomial kernel. The classification results for three datasets are represented in Tables 4-6. Ground truth map (GTM) beside the classification maps obtained by raw hyperspectral images and the hyperspectral images obtained by the super resolution methods are shown in Figs. 6-8. The following results can be concluded from the experiments:

1- ECNN and CNN methods provide the least classification accuracy in Indian and Pavia University datasets while the raw features and RES method achieve the lowest classification accuracy in Pavia center dataset.

2- The best performance is obtained by AGCNN and AEGCNN in Indian dataset, by AEGCNN and AGCNN in Pavia University dataset, and by AEGCNN and EGCNN in Pavia center dataset.

3- Generally, injection of Gabor features together with edge information or anomaly scores significantly improves quality of the super resolution performance, and so, the classification accuracy.

IV. CONCLUSION

Two Gabor based CNN methods are suggested for hyperspectral super resolution. The improved Gabor features weighted by anomaly scores are suggested to include anomalous pixels as valuable spatial details in the reconstructed image. The core structure of the proposed network consists of three convolutional blocks where each block contains two convolutional layers followed by ReLu and dropout layers. The edge feature cube and the weighted Gabor feature maps are

injected to output of the convolutional blocks through addition layer and concatenation layer, respectively. The proposed networks show significant improvement with respect to CNN, RES, Gabor based CNN and edge injected versions of them.

REFERENCES

[1] Banerjee, B. P., Raval, S., Cullen, P. J. 2020. UAV-hyperspectral imaging of spectrally complex environments, International Journal of Remote Sensing, 41 (11): 4136-4159.

[2] He, W., Chen, Y., Yokoya, N., Li, C., Zhao, Q. 2022. Hyperspectral super-resolution via coupled tensor ring factorization, Pattern Recognition, 122 (108280).

[3] Vivone, G. 2023. Multispectral and hyperspectral image fusion in remote sensing: A survey, Information Fusion, 89: 405-417.

[4] Imani, M., Ghassemian, H. 2020. An overview on Spectral and Spatial Information Fusion for Hyperspectral Image Classification: Current Trends and Challenges, Information Fusion, 59: 59–83.

[5] Kanatsoulis, C. I., Fu, X., Sidiropoulos, N. D., Ma, W. 2018. Hyperspectral Super-Resolution: A Coupled Tensor Factorization Approach," in *IEEE Transactions on Signal Processing*, 66 (24): 6503-6517.

[6] Simsek, M., Polat, E. 2021. Performance evaluation of pan-sharpening and dictionary learning methods for sparse representation of hyperspectral super-resolution. *SIViP* 15, 1099–1106.

[7] Tang, S., Xiao, L., Huang, W., Liu, P., Wu, H. 2015. Pan-sharpening using 2D CCA, Remote Sensing Letters, 6 (5): 341-350.

[8] Dixit, A., Agarwal, S. 2020. Super-resolution mapping of hyperspectral data using Artificial Neural Network and wavelet, Remote Sensing Applications: Society and Environment, 20 (100374).

[9] Dhara, S. K., Sen, D. 2019. Across-scale process similarity based interpolation for image super-resolution, Applied Soft Computing, 81 (105508).

[10] Fernandez-Beltran, R., Latorre-Carmona, P., Pla, F. 2017. Latent topic-based super-resolution for remote sensing, Remote Sensing Letters, 8 (6): 498-507.

[11] Lee, M. C., Chiu, S. Y., Chang, J. W. 2017. A Deep Convolutional Neural Network based Chinese Menu Recognition App, Information Processing Letters, 128: 14-20.

[12] Arun, P.V., Buddhiraju, K.M., Porwal, A., Chanussot, J. 2020. CNN based spectral super-resolution of remote sensing images, Signal Processing, 169 (107394).

[13] Wang, X., Ma, J., Jiang, J., Zhang, X.-P. 2021. Dilated projection correction network based on autoencoder for hyperspectral image super-resolution, Neural Networks.

[14] Hao, S., Wang, W., Ye, Y., Li, E., Bruzzone, L. 2018. A Deep Network Architecture for Super-Resolution-Aided Hyperspectral Image Classification With Classwise Loss, *IEEE Transactions on Geoscience and Remote Sensing*, 56 (8): 4650-4663.

[15] Wang, L., Bi, T., Shi, Y. 2020. A Frequency-Separated 3D-CNN for Hyperspectral Image Super-Resolution, *IEEE Access*, 8: 86367-86379.

[16] Dong, W., Zhou, C., Wu, F., Wu, J., Shi, G., Li, X. 2021. Model-Guided Deep Hyperspectral Image Super-

Resolution," in *IEEE Transactions on Image Processing*, 30: 5754-5768.

[17] Hammouche, R., Attia, A., Akhrouf, S., Akhtar, Z. 2022. Gabor filter bank with deep autoencoder based face recognition system, Expert Systems with Applications, 197 (116743).

[18] Ghassemi, M., Ghassemian, H., Imani, M. 2021. Hyperspectral Image Classification by Optimizing Convolutional Neural Networks based on Information Theory and 3D-Gabor Filters, International Journal of Remote Sensing, 42 (11): 4383–4413.

[19] Paoletti, M.E., Haut, J.M., Plaza, J., Plaza, A. 2019. Deep learning classifiers for hyperspectral imaging: A review, ISPRS Journal of Photogrammetry and Remote Sensing, 158: 279-317.

[20] Boggavarapu, L.N. P. K., Manoharan, P. 2020. A new framework for hyperspectral image classification using Gabor embedded patch based convolution neural network, Infrared Physics & Technology, 110 (103455).

[21] Imani, M. 2017. RX Anomaly Detector with Rectified Background, IEEE Geoscience and Remote Sensing Letters, 14 (8): 1313-1317.

[22] Han, X. -H., Chen, Y. -W. 2019. Deep Residual Network of Spectral and Spatial Fusion for Hyperspectral Image Super-Resolution, *2019 IEEE Fifth International Conference on Multimedia Big Data (BigMM)*, pp. 266-270.

[23] Liu, D., Li, J., Yuan, Q. 2021. A Spectral Grouping and Attention-Driven Residual Dense Network for Hyperspectral Image Super-Resolution, *IEEE Transactions on Geoscience and Remote Sensing*, 59 (9): 7711-7725.

[24] Vassilo, K., Taha, T., Mehmood, A. 2021. Infrared Image Super Resolution with Deep Neural Networks, *2021 11th Workshop on Hyperspectral Imaging and Signal Processing: Evolution in Remote Sensing (WHISPERS)*, pp. 1-5.

[25] Zhu, Z., Hou, J., Chen, J., Zeng, H., Zhou, J. 2021. Hyperspectral Image Super-Resolution via Deep Progressive Zero-Centric Residual Learning, *IEEE Transactions on Image Processing*, 30: 1423-1438.

[26] Yan, Q., Zhang, J., Feng, J. 2020. Spectral-Spatial Classification of Hyperspectral Image Using PCA and Gabor Filtering, *IGARSS 2020 - 2020 IEEE International Geoscience and Remote Sensing Symposium*, pp. 513-516.

[27] Imani, M. 2018. Anomaly detection from hyperspectral images using clustering based feature reduction, Journal of the Indian Society of Remote Sensing, 46(9):1389–1397.

[28] Imani, M. 2018. 3D Gabor Based Hyperspectral Anomaly Detection, AUT Journal of Modeling and Simulation, 50 (2): 189-194.

[29] Chang, C., Linin, C. 2008. *LIBSVM—A Library for Support Vector Machines*, [Online]. Available: http://www.csie.ntu.edu.tw/~cjlin/libsvm.

Ali Farajzadeh received his B.Sc. in Electronic Engineering from Urmia University, Urmia, Iran in 2001 and the M.Sc. and the Ph.D. degrees in Electronic Engineering from Zanjan University, Zanjan, Iran in 2009, and 2022 respectively. His research interests include Pattern Recognition, Image Processing and Remote Sensing.

Maryam Imani received her Ph.D. degree in Electrical Engineering, Communication, from Tarbiat Modares University, Tehran, Iran in 2015. She continued her research in Tarbiat Modares University as a Postdoc. Since 2018, she has been with Tarbiat Modares University in Tehran, Iran, where she is now the Associate Professor of Computer and Electrical Engineering. Her research interests include remote Sensing, Statistical Pattern Recognition, Signal and Image Processing, And Machine Learning.

Shahram Mohammadi received his B.Sc. in Electronic Engineering from Iran University of Science and Technology IUST in 1977, M.Sc. in Digital Techniques from Heriot-Watt University in UK in 1986 and Ph.D. in Fault-Tolerant Computing from Manchester University in 1990. From then on, he was working as a lecturer and researcher in Zanjan University. His research interests include Dependable Systems, Computer Networking and Pattern Recognition.